

Ring states in swarmalator systems

Kevin P. O’Keeffe

Senseable City Lab, Massachusetts Institute of Technology, Cambridge, Massachusetts 02139, USA

Joep H. M. Evers and Theodore Kolokolnikov

Department of Mathematics and Statistics, Dalhousie University, Halifax B3H 4R2, Canada

(Received 31 August 2017; revised manuscript received 14 April 2018; published 7 August 2018)

Synchronization is a universal phenomenon, occurring in systems as disparate as Japanese tree frogs and Josephson junctions. Typically, the elements of synchronizing systems adjust the phases of their oscillations, but not their positions in space. The reverse scenario is found in swarming systems, such as schools of fish or flocks of birds; now the elements adjust their positions in space, but without (noticeably) changing their internal states. Systems capable of both swarming and synchronizing, dubbed swarmalators, have recently been proposed, and analyzed in the continuum limit. Here, we extend this work by studying finite populations of swarmalators, whose phase similarity affects both their spatial attraction and repulsion. We find ring states, and compute criteria for their existence and stability. Larger populations can form annular distributions, whose density we calculate explicitly. These states may be observable in groups of Japanese tree frogs, ferromagnetic colloids, and other systems with an interplay between swarming and synchronization.

DOI: [10.1103/PhysRevE.98.022203](https://doi.org/10.1103/PhysRevE.98.022203)

I. INTRODUCTION

Synchronization is a well studied [1–4] phenomenon spanning many disciplines. In biology it is seen in discharging pacemaker cells [5,6], coherently flashing fireflies [7,8], and accordantly croaking tree frogs [9–11]. In chemistry it is seen in the metabolic cycles of yeast cells [12], and in physics, in arrays of Josephson junctions [13], power grid dynamics [14], and even the wobbling of the millenium bridge [15].

In synchronizing systems, the dynamic state variables are the oscillators’ phases, whose influence on each other leads to macrolevel temporal structures (synchrony). A similar effect occurs in swarming [16–25], a phenomenon as widespread as synchronization, as evidenced by flocks of birds [26,27], locust swarms [28–30], bacterial aggregation [31–33], schools of fish [34,35], predator-prey interactions [36,37], self-assembly [38–42], and even the vortices of Bose-Einstein condensates [43–47]. Like synchronizing oscillators, the interactions between swarming particles give rise to group-level structures. But, now the (dynamic) state variables are the individuals’ positions, and the structures formed are spatial.

Viewed this way, swarming and synchronization are strikingly similar. Both are canonical examples of emergent phenomena. Both are dizzyingly pervasive, occurring in far-flung settings like the menstrual cycle [48] and quantum gases [47]. Yet in spite of these commonalities, the two fields have developed largely independently. In swarming the units are mobile, but do not have internal dynamics. In synchronization the situation is reversed: the oscillators have internal dynamics, but do not move through space.

Recently, however, researchers in both fields have started to study systems with both spatial and internal dynamics. From the swarming side, von Brecht and Uminsky [42] have endowed aggregating particles with an internal polarization

vector. In the sync community, researchers have considered mobile oscillators when modeling robotics and biological phenomena [49–53]. In these works, however, the coupling between the space dynamics and the phase dynamics is only one way: their phase evolution is influenced by their relative distances, but their relative phases do *not* affect their movements.

Oscillators whose space dynamics and phase dynamics are bidirectionally coupled have also been considered. The pioneering work was done by Tanaka *et al.* [54–56] when studying “chemotactic oscillators,” oscillators whose movements and interactions are mediated by a surrounding chemical. They studied a very general model, from which they derived reduced dynamics using center manifold and phase reduction techniques. More recent works have been carried out by Starnini *et al.* [57], and O’Keeffe *et al.* [58], who took a bottom-up approach. They defined minimal, toy models which enabled greater tractability. The latter called the elements of their system “swarmalators” to highlight their twin identities as swarming oscillators, and to distinguish them from the “mobile oscillators” of the preceding paragraph, whose motion evolves independently of their phase.

Defined this way, swarmalators are, to our knowledge, hypothetical entities. By this we mean there are no real world systems which unequivocally display the required two-way, space-phase coupling. That said, there are some promising candidates. For example, tree frogs, crickets, and katydids are known to synchronize their calling rhythms with others close to them in space (making the phase dynamics position dependent) [59,60]. Perhaps, as some believe [61], the relative phases of their calls also affect their movements, which would complete the requisite feedback loop between the space dynamics and the phase dynamics.

Another contender is biological microswimmers, such as bacteria, algae, or sperm. Here, the phase variable is associated with the rhythmic wriggling of the swimmer's tail. Since this wriggling both affects, and is affected by, the local hydrodynamic environment, it seems likely that the behavior of neighboring sperm would be coupled. Whether this coupling is truly bidirectional is yet to be determined. That said, there is evidence that sperm, at least, behave this way. As discussed in [62], neighboring sperm can synchronize their wriggling, which in turn is thought to enhance their mutual spatial attraction.

Myxobacteria also have the right ingredients to be swarmalators. In this case, the phase variable is an internal, cyclic degree of freedom, which has been theorized to influence their motion, and vice versa [63]. The same is true of colloidal Janus particles, where now the phase corresponds to an oscillation about the center of mass (which occurs in response to an external magnetic field). Here again, the physics is such that the oscillations and movements of the particles are mutually dependent on each other, as required of swarmalators [64].

In this work, we contribute to the theoretical study of swarmalators. We study two realistic modifications of the model defined in [58]. The first is the effect of finite population sizes (in [58] continuum arguments were used), which we show lead to stable ring states. The second is a change in length scale of the space-phase coupling. In [58] this length scale was chosen to be the same as that of the spatial attraction. However, in some swarmalator systems, such as magnetic Janus particles [64] and Japanese tree frogs [11], this space-phase interaction occurs at the length scale of the spatial repulsion. We here account for this effect by allowing phase similarity to affect both spatial attraction and spatial repulsion.

II. MODEL

We consider swarmalators confined to move in two spatial dimensions

$$\dot{\mathbf{x}}_k = \frac{1}{N} \sum_{j=1}^N [\mathbf{I}_1(\mathbf{x}_j - \mathbf{x}_k) F_1(\theta_k - \theta_j) + \mathbf{I}_2(\mathbf{x}_j - \mathbf{x}_k) F_2(\theta_k - \theta_j)], \quad (1)$$

$$\dot{\theta}_k = \omega_k + \frac{K}{N} \sum_{j=1}^N H(\theta_j - \theta_k) G(|\mathbf{x}_j - \mathbf{x}_k|) \quad (2)$$

for $k = 1, \dots, N$, where N is the population size and $\mathbf{x}_k \in \mathbb{R}^2$. $\theta_k \in \mathbb{S}^1$ is the phase of the k th swarmalator while its natural frequency is ω_k . The spatial attraction and repulsion between swarmalators are represented by $\mathbf{I}_1, \mathbf{I}_2 \in \mathbb{R}^2$. (Depending on the sign of F_1, F_2 , however, this can change, and \mathbf{I}_1 can be repulsive and/or \mathbf{I}_2 can be attractive. We discuss when this occurs later.) The phase interaction is encoded by $H \in \mathbb{R}$, and the influence of phase similarity on spatial attraction and repulsion is captured by the functions $F_1, F_2 \in \mathbb{R}$. Finally, the function $G \in \mathbb{R}$ represents the influence of spatial proximity on the phase dynamics.

Consider the following instance of this model:

$$\dot{\mathbf{x}}_k = \frac{1}{N} \sum_{j \neq i}^N (\mathbf{x}_j - \mathbf{x}_k) (A + J_1 \cos(\theta_j - \theta_k)) - (B - J_2 \cos(\theta_j - \theta_k)) \frac{\mathbf{x}_j - \mathbf{x}_k}{|\mathbf{x}_j - \mathbf{x}_k|^2}, \quad (3)$$

$$\dot{\theta}_k = \frac{K}{N} \sum_{j \neq i}^N \frac{\sin(\theta_j - \theta_k)}{|\mathbf{x}_j - \mathbf{x}_k|^2}. \quad (4)$$

We choose a linear attraction kernel and power law repulsion, as is common in studies of the aggregation model [25,65], because it simplifies the analysis. Specifically, in the absence of space-phase coupling, $J_1 = J_2 = 0$, this choice of $\mathbf{I}_1, \mathbf{I}_2$ causes swarmalators to form disks of uniform density in space. We note the term $\mathbf{x}_j - \mathbf{x}_k$ indicates the k th swarmalator is attracted to the j th swarmalator only when the term $[A + J_1 \cos(\theta_j - \theta_k)]$ is positive. If the latter term is negative, we have the reverse scenario, where the k th swarmalator is *repelled* from the j th swarmalator [similar statements hold for the terms $(\mathbf{x}_j - \mathbf{x}_k)/|\mathbf{x}_j - \mathbf{x}_k|^2$ and $B - J_2 \cos(\theta_j - \theta_k)$]. Again for simplicity, we both choose the sine function for H , and consider identical swarmalators $\omega_k = \omega$. By a change of reference frame we set $\omega = 0$ without loss of generality. Finally, by rescaling time and space we set $A = B = 1$. Note this implies $(J_1, J_2) \rightarrow (\tilde{J}_1, \tilde{J}_2) = (J_1/AB, J_2/AB)$, but for notational convenience we drop the tilde notation. This leaves three parameters (J_1, J_2, K) .

The parameter K measures the strength of the phase coupling. For $K > 0$, the phase coupling between swarmalators tends to minimize their phase difference, while for $K < 0$, it tends to maximize it. The parameters $J_1, J_2 > 0$ measure the extent to which phase similarity influences spatial attraction and repulsion, respectively. For $0 < J_1, J_2 < 1$, the functions F_1 and F_2 are strictly positive. Then, the phase similarity enhances just the *magnitude* of $\mathbf{I}_1, \mathbf{I}_2$. However, for $J_1, J_2 > 1$, F_1, F_2 can change sign (depending on the value of $\theta_j - \theta_k$). As we discussed earlier, this means the functions $\mathbf{I}_1, \mathbf{I}_2$ become repulsive and attractive, respectively.

We remark that J_2 does not appear in [58], which meant phase similarity affected spatial attraction, but not spatial repulsion. We here include it for greater generality, so that our results may be applied to swarmalators whose space-phase coupling occurs on the length scale of the spatial repulsion, as is the case, for example, for magnetic Janus particles [64,66] and Japanese tree frogs [9,11]. We also remark that in [58] $G(|\mathbf{x}|) = 1/|\mathbf{x}|$, but we choose $G(|\mathbf{x}|) = 1/|\mathbf{x}|^2$ here because it simplifies the analysis.

III. RESULTS

A. Ring phase waves

Simulations show that for certain parameter values, a stationary state is formed where the swarmalators arrange themselves in a ring centered about the origin, with their phases perfectly correlated with their spatial angle (i.e., $\theta_k = \phi_k + \text{const}$, where ϕ_k is angle between \mathbf{x}_k and the positive x axis). Accordingly, we call this state the *ring phase wave* and plot it in Fig. 1(a). We now analyze this state.

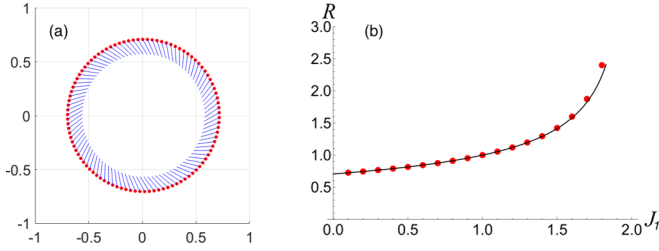


FIG. 1. (a) Scatter plot of a stable ring phase wave state in the (x, y) plane. The phase of each swarmalator is represented by a blue ray, and corresponds to the angle the ray makes with the positive x axis. As can be seen, in this state the spatial angle $\phi_k = \tan^{-1}(y_k/x_k)$ of each swarmalator is correlated with its phase (i.e., $\phi_k = \theta_k + \text{const}$). Parameter values were $J_2 = 1$, $J_1 = 0$, $K = -0.003$, and $N = 100$. (b) Radius of ring state versus J_1 . Red dots show simulation results for $J_2 = 1$ and $N = 100$. The black curve shows theoretical prediction (7). To produce the data for the plot, we integrated the equations of motion (3) and (4) using Euler's method until the steady state was reached.

Existence. In the ring phase wave state the position and phase of the k th swarmalator are

$$\mathbf{x}_k = R \cos(2\pi k/N)\hat{x} + R \sin(2\pi k/N)\hat{y}, \quad (5)$$

$$\theta_k = 2\pi k/N + C, \quad (6)$$

where R is the radius of the ring, \hat{x} , \hat{y} are unit vectors in the (x, y) directions, $N > 1$, and the constant C is determined by the initial conditions. After substituting the *Ansätze* (5) and (6) into the equations of motion (3) and (4), and after algebraic manipulation, we derive the following expression for the radius:

$$R = \sqrt{\frac{N-1+J_2}{N(2-J_1)}} \quad (7)$$

which is valid for any value of the coupling constant K . For large N this becomes $R \sim \sqrt{1/(2-J_1)}$, independent of J_2 . This expression for radius of the ring agrees with simulation as shown in Fig. 1(b). By requiring the argument of the square root be positive, we see rings which satisfy the *Ansätze* (5) and (6) exist in the parameter region $\{J_1 < 2, J_2 > 1 - N\} \cup \{J_1 > 2, J_2 < 1 - N\}$.

Stability when $\mathbf{K} = \mathbf{0}$. The above analysis proves the existence of ring phase wave, but not their stability, which we here investigate. For simplicity, we start with the case $K = 0$ so that swarmalators' phases are "frozen" at the values defined by (6). In Appendix B we show that the ring phase wave is stable for $J_1 \in (J_{1a}, 2)$ where

$$J_{1a} := \begin{cases} 2 - 8 \frac{(N-1+J_2)}{(N-2)^2(1-J_2)}, & N \text{ even, } N > 4 \\ 2 - 8 \frac{(N-1+J_2)}{(N-1)(N-3)(1-J_2)}, & N \text{ odd, } N > 4. \end{cases} \quad (8)$$

For $J_1 < J_{1a}$ (and $K = 0$ remember) the ring becomes unstable. However, it does not break up entirely. Instead, it "fattens" slightly, while the phase distribution remains unchanged. This is depicted in snapshot D in Fig. 2. The destabilizing mode in this case is the highest frequency wave number $\lfloor N/2 \rfloor$.

We remark that the case $J_2 = J_1 = 0$ has a connection to vortex dynamics. In a classic paper [67], the stability of ring configurations of fluid vortices was studied, whose motion is controlled by the classic Helmholtz equations. It turns out that the motions of the center of masses of the vortices obey the aggregation equation. That is, our governing equations (3) and (4) with $J_1 = J_2 = 0$. In other words, the vortices swarm. In [68] the stability of ring states was studied, and it was found that six or less vortices in the classical vortex equations are stable, seven are neutral (borderline stable or unstable), and eight or more are unstable. This is consistent with our result (8) since $J_{1a} = 0$ at $N = 7$ and $J_2 = 0$.

Stability when $\mathbf{K} > \mathbf{0}$. When K is positive, the swarmalators' phases are no longer frozen. Instead, they tend to synchronize with that of their neighbors. This makes ring states unstable. A mode-two instability is triggered (which we have determined by numerically computing the eigenvectors), which leads to the "elliptization" of a thin annulus, as shown in snapshot F of Fig. 2. This is followed by either a perfectly synchronous, static crystal formation (equivalent to the "static sync" state in [58]) or by a blowup, where the swarmalators escape to infinity. Which of these two states is realized appears (i.e., indicated by numerics) to be parameter dependent (as opposed to depending on initial conditions). Numerics suggest the critical value is at $J_1 \approx 1$ (for $J_2 = 0$) although a theoretical result is lacking.

Stability when $\mathbf{K} < \mathbf{0}$. Negative values of K are more interesting. Now, neighboring swarmalators tend to desynchronize their phases. Do rings states persist in this case? In Appendix B we show they do, provided $J_1 > J_{1b}$ and $K \in (K_{\text{Hopf}}, 0)$ where

$$J_{1b} = \begin{cases} 2 \left(\frac{1}{1-\frac{4}{N^2}} \right) - \frac{1}{1-J_2} \frac{8}{(N-\frac{4}{N})}, & N \text{ even, } N > 4 \\ 2 \left(\frac{1}{1-\frac{4}{N^2-1}} \right) - \frac{1}{1-J_2} \frac{8}{(N-\frac{5}{N})}, & N \text{ odd, } N > 4 \end{cases} \quad (9)$$

and

$$K_{\text{Hopf}} = \begin{cases} -\frac{(J_2-1)(-2+J_1)N^2+(-4J_2+4)J_1+8J_2]N+4J_1(J_2-1)}{N(N-4)(2-J_1)} \\ -\frac{(J_2-1)(-2+J_1)N^2+(-4J_2+4)J_1+8J_2]N+(3J_2-3)J_1+2J_2-2}{(N^2-4N-1)(2-J_1)}, \end{cases} \quad (10)$$

where the top equation is for N even, and the bottom is for N odd. As before, these both require $N > 4$.

These instability boundaries are drawn in Fig. 2. Notice that $J_{1a} < J_{1b}$, so J_{1b} is the critical parameter value when $K < 0$. Notice also that there are two ways for rings to become unstable. The first is by holding K constant, and decreasing J_1 below J_{1b} (moving horizontally in Fig. 2). This corresponds to a saddle-node bifurcation, and the ring again fattens, like when $K = 0$. But the similarity (to the scenario when $K = 0$) is not exact; here the phase distribution gets distorted (recall it remained unchanged when $K = 0$), as shown in snapshot E of Fig. 2.

Rings also become unstable when J_1 is held constant, and K is decreased past $K_{\text{Hopf}} < 0$ (moving vertically in Fig. 2). As indicated by the subscript, this leads to a Hopf bifurcation. The ring structure is completely destroyed, and a disordered gaslike state forms as illustrated in snapshot G of Fig. 2. In this state, the swarmalators move erratically in space and are

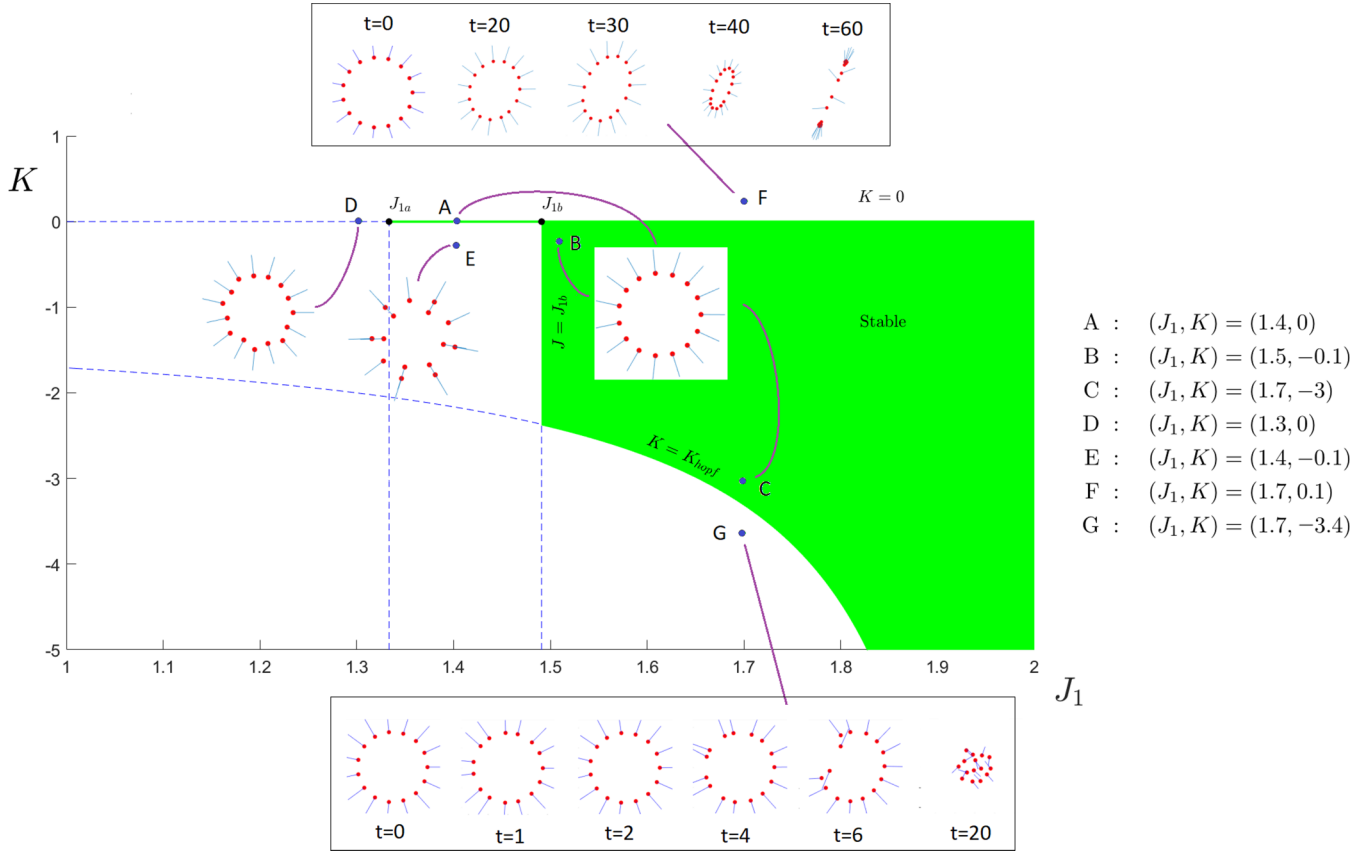


FIG. 2. Stability diagram for the ring phase wave state in (J_1, K) space with $N = 15$, $J_2 = 0$. Stable regions are indicated with a green color. Insets show the solution to Eqs. (3) and (4) corresponding to parameter values as shown (A through G) as scatter plots in the (x, y) plane. The phase of each swarmalator is represented by a blue ray, and corresponds to the angle the ray makes with the positive x axis. Initial conditions were taken to be a ring of radius 1, slightly perturbed. The ring is stable for parameter values A,B,C.

desynchronized with each other. In the continuum limit these movements die out and the “static async” state reported in [58] is achieved, in which the swarmalators form an asynchronous disk of uniform density and radius 1.

We pause to summarize our results so far. We have computed existence and stability criteria for ring states, displayed in the (J_1, K) plane (with $J_2 = 0$ and $N = 15$) in Fig. 2, and discussed the possible bifurcations. We close this section of ring phase wave states by noting some interesting features of the expressions for J_{1a} , J_{2a} , K_{Hopf} .

The first is their scaling with the population size N . For any N , it can be shown that $J_{1b} > J_{1a}$. Therefore, with $K < 0$ held fixed, and J_1 gradually decreased, J_{2a} will be crossed first and the instability changing the phase distribution (snapshot E) will be triggered. When J_{1a} is crossed after this, the instability shown in snapshot D will be triggered. However, as $N \rightarrow \infty$, both $J_{1a} \sim J_{1b} \sim 2 - \frac{8}{1-J_2}$, which means that the two instabilities happen nearly simultaneously!

The second interesting feature of the expressions for J_{1a} , J_{2a} , K_{Hopf} is that they can be reversed to find $N(J_1, J_2, K_{\text{Hopf}})$, allowing us to treat N as a bifurcation parameter. This lets us determine the maximum number of swarmalators in a ring which we define as

$$N_{\text{max}} := \text{largest } N \text{ such that } J_1 > J_{1b}. \quad (11)$$

Then, the ring is stable for all $N < N_{\text{max}}$ as long as K is sufficiently small, namely, $K \in (K_{\text{Hopf}}(N_{\text{max}}), 0]$. When N is large, we can rearrange Eq. (10) to obtain

$$N_{\text{max}} \sim \frac{8}{(2 - J_1)(1 - J_2)}. \quad (12)$$

We restate that the above equation is valid only for large N , which means either $0 < 2 - J_1 \ll 1$ or $0 < 1 - J_2 \ll 1$. We see from (12) that N_{max} increases with increasing J_1 and J_2 . Or, put another way, swarmalators can form larger rings than regular swarming particles (which have no internal degree of freedom); the inclusion of the phase variable stabilizes the ring state.

The last feature of interest is a special parameter value, $J_2 = 1$, where rings are unusually stable. To see why, we let $J_2 \rightarrow 1^-$ in (8), (9), and (10) and find

$$J_{1a}, J_{2a} \rightarrow -\infty, \quad (13)$$

$$K_{\text{Hopf}} \rightarrow \begin{cases} -\frac{8}{(N-4)(2-J_1)}, & N \text{ even, } N > 4, J_2 = 1 \\ -\frac{8}{(N-4-1/N)(2-J_1)}, & N \text{ odd, } N > 4, J_2 = 1. \end{cases} \quad (14)$$

Consequently, when $J_2 = 1$, $J_1 < 1$, and $K \in (K_{\text{Hopf}}, 0]$ the ring phase wave state is stable for *any* N ! Furthermore, its radius is finite, and independent of N . This remarkable fact is

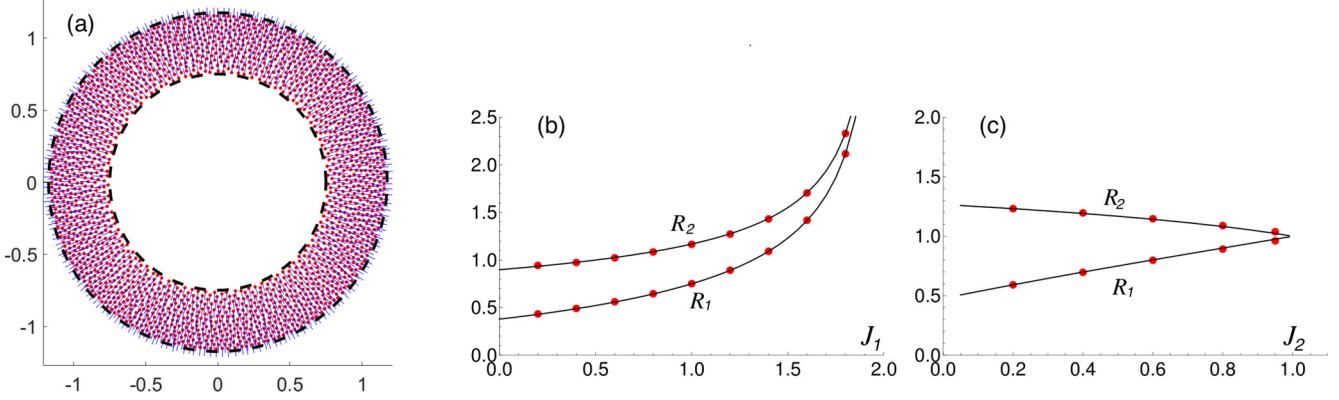


FIG. 3. The annular phase wave state. (a) Scatter plot of annular phase wave state in (x, y) plane. The phase of each swarmalator is represented by a blue ray, and corresponds to the angle the ray makes with the positive x axis. Data were collected by solving Eqs. (3) and (4) using the Euler method with $J_1 = 0.5$, $J_2 = 1$, $K = 0$, and $N = 2 \times 10^3$ swarmalators. Asymptotic predictions for the inner and outer radii, as given by the roots of (17) and (18), were $R_1 = 0.7504$, $R_2 = 1.16834$, and are indicated by dashed curves. Swarmalators were initially placed in a ring and their initial phases were $\tan^{-1}(y_k/x_k)$. (b) Comparison of numerics and asymptotic computations of R_1 and R_2 for $J_2 = 0.5$ and with varying J_1 . (c) $J_1 = 1.0$ and J_2 is varied.

demonstrated in Fig. 1(a), where a ring of $N = 100$ particles is observed to be stable.

We note that for $J_2 > 1$, simulations show that the particles exhibit finite-time collisions as N is increased. We therefore restrict our analysis to the parameter region $J_2 < 1$. Thus, aside from the special case $J_2 = 1$, the ring is stable for $N < N_{\max}$. For $N > N_{\max}$ it bifurcates into either the annular phase wave state or the splintered phase wave state, which we discuss next.

B. Annular phase waves

When $N > N_{\max}$ and $K = 0$ the swarmalators form an annular distribution where their spatial angle is perfectly correlated with their phase, plotted in Fig. 3(a). This state was reported in [58], where it was named the “static phase wave.” To distinguish this state from the ring phase waves of the previous section, we here refer to it as the “annular phase wave.”

We explicitly solve for the density of the annular phase wave in the continuum limit $N \rightarrow \infty$. Let $\rho(\mathbf{x}, \theta, t)$ denote the density of swarmalators, where $\rho(\mathbf{x}, \theta, t) d\mathbf{x} d\theta$ gives the fraction of swarmalators with positions between \mathbf{x} and $\mathbf{x} + d\mathbf{x}$ and phases between θ and $d\theta$ at time t . We then use the following *Ansatz*:

$$\rho(r, \phi, \theta, t) = \frac{1}{2\pi} g(r) \delta(\phi - \theta), \quad R_1 \leq r \leq R_2 \quad (15)$$

where (r, ϕ) are polar coordinates and $g(r)$, R_1 , R_2 are unknown. In Appendix B we solve for $g(r)$ by substituting (15) into the continuity equation and deriving an integral equation for $g(r)$. We then reduce this integral equation to a second order ordinary differential equation (ODE), whose solution is

$$g(r) = C_1 r^{-\frac{1}{\sqrt{1-J_2}}-2} + C_2 r^{\frac{1}{\sqrt{1-J_2}}-2} + \frac{6}{3-4J_2}, \quad (16)$$

where C_1, C_2 are complicated expressions involving R_1, R_2, J_1, J_2 given by Eqs. (B20) and (B21). Note this is valid for $J_2 \neq \frac{3}{4}$. At this parameter value, $g(r)$ takes a different functional form, which we display and discuss in Appendix B.

We also derive implicit equations for the inner and outer radii R_1, R_2 in terms of J_1, J_2 :

$$h_1(R_1, R_2, J_1, J_2) = 0, \quad (17)$$

$$h_2(R_1, R_2, J_1, J_2) = 0, \quad (18)$$

where h_1, h_2 are complicated expressions given by Eqs. (B26) and (B27). We solved these using *Mathematica*. The results are shown in Figs. 3(b) and 3(c), which agree well with numerics.

Notice in Fig. 3 that $R_1 \rightarrow R_2$ as $J_1 \rightarrow 2$ in panel (b) and $J_2 \rightarrow 1$ in panel (c), indicating the morphing of the annular phase wave into the ring phase wave state. We analytically confirm $J_{2c} = 2$ by substituting $R_1 = R_2$ into (17). The result is

$$(3 - 4J_2)(-1 + J_2 + \sqrt{1 - J_2})R_2^{\frac{2}{\sqrt{1-J_2}}} = 0. \quad (19)$$

From this we see $-1 + J_2 + \sqrt{1 - J_2} = 0$ which gives

$$J_{2c} = 1. \quad (20)$$

Note (19) is only valid for $J_2 \neq \frac{3}{4}$, a property inherited from the expression for $g(r)$ (see Appendix B). We confirm the J_{1c} value similarly; we substituted $R_1 = R_2 - \delta$ into (18) and took a series expansion for small δ leading to

$$(J_1 - 2)(4J_2 + 3)(-J_2 + \sqrt{J_2 + 1} - 1) \times \left(\frac{J_2 + \sqrt{(J_2 + 1)^2 + 1}}{\delta} \right)^{\frac{2}{\sqrt{J_2+1}}} = 0 \quad (21)$$

from which we see

$$J_{1c} = 2. \quad (22)$$

We close by distilling our results. We explicitly solved for the density in the annular phase wave state, and showed it exists in the parameter region $0 < J_1 < 2$, $0 < J_2 < 1$. As the extremal edges of this region are approached, the annulus gets thinner and thinner until the ring phase wave is achieved right at the boundary $J_1 = 2$ or $J_2 = 1$. When $J_1 = 2$, the radius of the ring approaches ∞ , whereas when $J_1 \rightarrow 2^-$ it

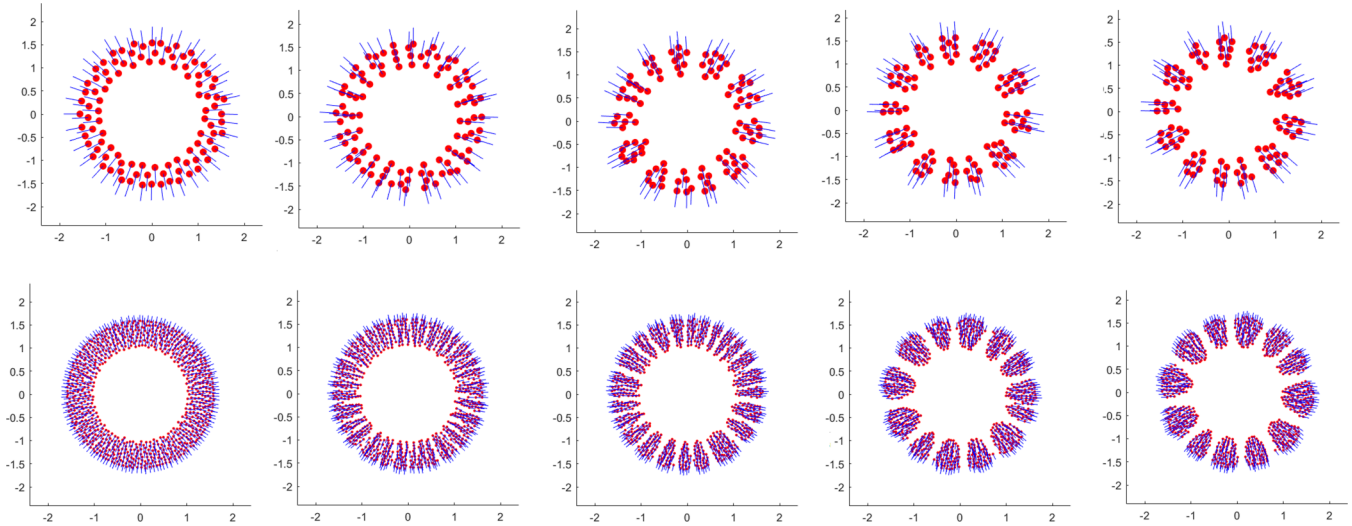


FIG. 4. Bifurcation of an annulus into a splintered phase wave with 12 clusters. Panels show snapshots of the systems at the different (increasing) times. Data were collected by integrating the governing equations (3) and (4) using the Euler method. Swarmalators are illustrated as points in the (x, y) plane, whose phase is represented by angle the blue ray makes with the positive x axis. Top row: parameter values are $J_1 = 1.5$, $J_2 = 0$, $K = -0.05$, $N = 100$, and reading from left to right, the times of each panel are $t = 60, 331.6, 1940, 6940.2, 101830$. Bottom row: $J_1 = 1.5$, $J_2 = 0$, $K = -0.05$, $N = 100$, and times $t = 5, 95, 205.2, 9785, 18415$. Note, for smaller values of N , the system takes longer to equilibrate, and the boundaries between clusters become less well defined.

remains finite. Note that we have only proved the *existence* of the annular phase wave here, and make no claims about its stability. Numerics indicate that it is stable, but a proof is beyond the scope of this work.

C. Splintered phase wave

In the above section we showed that when $K = 0$ and $N > N_{\max}$, the ring phase wave bifurcates into the annular phase wave. For $K < 0$, they bifurcate into a new state called the *splintered phase wave*, previously reported in [58]. Here, the ring “splinters” into disconnected clusters of distinct phase. Within each cluster, swarmalators “quiver,” executing small cycles in both position and phase about their mean values. We showcase the evolution of this state from the annular phase wave in Fig. 4.

This nonstationary behavior makes analysis difficult, and we were unable to construct the state or determine its stability. We were, however, able to heuristically find an upper bound for the number of clusters that form. We did this by leveraging our analysis for the ring states: we naively pictured each cluster as a single particle, which lets us reimagine the splintered phase wave state as a ring state. We then use our previous analysis to estimate N_{\max} given by (11). For example, for parameter values used in Fig. 4, $N_{\max} = 15$, whereas the number of observed clusters is 12 or 13. Simulations at other parameter values have the same behavior.

D. Genericity

So far, our analysis has been for the instance (3), (4) of the model (1), (2). We here check if the phenomena we found are generic to the model, rather than specific to the instance of the model. We do this by exploring the effects of different functional forms for \mathbf{I}_1 , \mathbf{I}_2 , F , G . We study three such choices, listed below. In all cases we found the same states enumerated

in Fig. 2. We exhaustively show these states for all three choices of interaction function in Fig. 7 in Appendix C:

$$\mathbf{I}_1, \mathbf{I}_2, G, H = \frac{\mathbf{x}}{|\mathbf{x}|^2}, \frac{\mathbf{x}}{|\mathbf{x}|^4}, \frac{1}{|\mathbf{x}|}, \sin \theta, \quad (23)$$

$$\mathbf{I}_1, \mathbf{I}_2, G, H = \mathbf{x}e^{-|\mathbf{x}|}, \frac{\mathbf{x}}{|\mathbf{x}|^2}, \frac{1}{|\mathbf{x}|}, \sin \theta, \quad (24)$$

$$\mathbf{I}_1, \mathbf{I}_2, G, H = \mathbf{x}, \frac{\mathbf{x}}{|\mathbf{x}|^2}, \frac{e^{-|\mathbf{x}|}}{|\mathbf{x}|^2}, \sin \theta. \quad (25)$$

We were also curious if the ring state would persist in the presence of heterogeneity. To this end, we imbued swarmalators with natural frequencies ω_k linearly spaced on $[-\omega_0, \omega_0]$ (recall so far we have considered identical swarmalators $\omega_i = \omega = 0$, the zero value achieved by a change of reference). Simulations show the ring distribution persists, but now the swarmalators split into counter-rotating groups (which follows from the fact that $\langle \dot{\theta}_i \rangle = \langle \dot{x}_i \rangle = 0$ in our model). That is, individual swarmalators execute circular motion in both space and phase, with the overall *density* of swarmalators remaining constant. This state is equivalent to the active phase wave reported in [58], with the inner and outer radii of the annular being the same. Figure 5 displays the state in the (x, y) plane. A theoretical understanding of this state is lacking [aside from the trivial result that the radius of the ring is still given by (7)], and is left for future work.

IV. DISCUSSION

We studied the stability of ring states in swarmalator systems with both phase-dependent attraction and phase-dependent repulsion. We analytically computed criteria for their existence and stability, which were valid for all population sizes N . We found that in general (even for K sufficiently small and negative) ring states are stable for sufficiently small

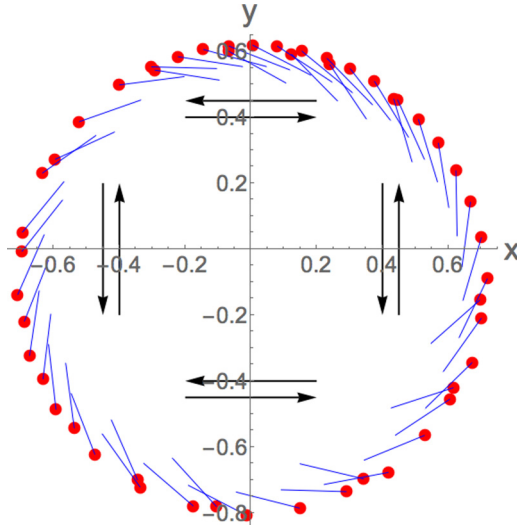


FIG. 5. Ring state in the presence of heterogeneous natural frequencies $\omega_k = \omega_0 + (2k\omega_0)/(N - 1)$ with $\omega_0 = 0.2$, $N = 50$ and $k = 1, 2, 3, \dots$. We used the Euler method with step size $dt = 0.1$. The ring distribution remains, but swarmalators are no longer stationary; they split into counter-rotating (in both space and phase) groups, as indicated by the black arrows. This shearlike flow was reported in [58], where it was named the active phase wave state.

populations $N < N_{\max}$. For $N > N_{\max}$, they bifurcate into either the annular phase wave or splintered phase wave state. We constructed the former state in the continuum limit $N \rightarrow \infty$, but its stability remains an open problem. We were unable to construct the latter state, or determine its stability, and so these are also open problems. We were, however, able to heuristically derive an upper bound for the number of synchronous clusters which comprise the state.

Ring states have been previously studied in “regular” swarming systems, where particles have a position x_k but no internal phase θ_k . They were first shown to be stable in two dimensions [41,69], and later in three [39,40]. The general case of n dimensions was completed in [70], where the authors showed that the formation of rings depends on the strength of the near-field repulsion (more precisely, they show the support of the local minimizer of the interaction potential has Hausdorff dimension greater than or equal to the strength of the repulsion at the origin). This means rings can only form when the repulsion between two particles is bounded (i.e., no hard shell repulsion). Interestingly, we have demonstrated this is not true for swarmalators: our repulsion term was hard shelled [see Eq. (3)], yet we proved rings are stable for certain parameter values (detailed in Fig. 2).

A similar result is found in anisotropic swarming systems, where the particles now have an additional state variable such as an orientation or a heading vector. For example, von Brecht and Uminsky [42] used an anisotropic version of the aggregation equation in 3D to explore the effects of polarization on molecular structures, and found that anisotropy enhanced the stability of “blackberries,” shell-like structures found in biochemical contexts. This echoes our finding that the inclusion of a phase in swarming systems stabilizes ring states. It seems the addition of a circular state variable (for

swarmalators an internal phase, and for swarming particles an orientation or heading) stabilizes structures of low co-dimension (rings or shells). Rigorously justifying this claim is an interesting open problem; perhaps an extension of the techniques used in [70] could prove fruitful.

An apposite future goal would be to find or manufacture the states we studied here in the real world. States similar to the rings and static phase wave have been realized in ferromagnetic colloids confined to liquid-liquid interfaces. So called “asters” consist of annular structures of particles whose magnetic dipole vectors correlate with their spatial angle [71], as happens in the ring and static phase wave states studied here. Ringlike states are also found in groups of Japanese tree frogs, who congregate along edges of paddy fields [10]. The phase distribution is, however, different to that found here; instead, neighboring frogs are perfectly out of phase with each other. Full phase waves are yet to be discovered.

There are also theoretical avenues for future work within our proposed model of swarmalators. For instance, we considered motion in just two spatial dimensions. While there are some physical systems where this type of motion is realized, such as certain active colloids [72] or sperm, which are often attracted to the surface of liquids [73], this was mostly for mathematical convenience. The more realistic case of motion in three spatial dimensions would be interesting to explore. For instance, 3D analogs of the states found in 2D were reported in [58], but their stability was not analyzed. Moreover, finite populations sizes were unexplored. Perhaps the analysis in [42] would be helpful in answering these questions.

Other extensions include adding heterogeneity in the coupling parameters K , J_1 , J_2 , and the natural frequencies ω_k , or considering delayed or noisy interactions. Less trivial phase dynamics could also be interesting. As we stated, the choice of $H(\theta) = \sin(\theta)$ was inspired by the Kuramoto model [74], but leads to trivial phenomena in the $K > 0$ plane (total synchrony). Perhaps using the more realistic Winfree model [3], which has richer phase dynamics, would lead to more interesting swarmalator phenomena when K is positive.

ACKNOWLEDGMENTS

Research was supported by NSF Grants No. DMS-1513179 and No. CCF-1522054 (K.P.O.) and NSERC Discovery Grant No. RGPIN-33798 and Accelerator Supplement Grant No. RGPAS/461907 (T.K. and J.H.M.E).

APPENDIX A: STABILITY OF RING PHASE WAVE

Here, we develop the stability theory for ring states of the swarmalator model defined in the main text, using techniques similar to those developed in [41,69,75,76]. It is convenient to use complex notation to describe the ring phase wave state. We thus identify the real, two-dimensional, vector $\mathbf{x}_k = (x_k^{(1)}, x_k^{(2)})$ as a point in the complex plane (so that $x_k^{(1)}$ is real part of the complex number, and $x_k^{(2)}$ is the imaginary part). To remind ourselves that \mathbf{x}_k is now a complex number, we drop the bold notation hereafter.

We first consider a more general model of the form

$$x'_k = \sum_j f(|x_k - x_j|^2)(x_k - x_j) + \sum_j \cos(\theta_k - \theta_j)h(|x_k - x_j|^2)(x_k - x_j), \quad (\text{A1})$$

$$\theta'_k = \sum_j \sin(\theta_k - \theta_j)g(|x_k - x_j|^2). \quad (\text{A2})$$

The model defined by Eqs. (3) and (4) then corresponds to the specific choice

$$f(r) = \frac{1}{r} - 1; \quad h(r) = -\frac{J_2}{r} - J_1, \quad g(r) = -\frac{K}{r}. \quad (\text{A3})$$

The ring phase wave steady state is given by

$$x_k = Rz^k, \quad \text{where } z := \exp(2\pi i/N), \quad \theta_k = 2\pi k/N,$$

where R is the ring radius. This *Ansatz* satisfies Eq. (A2) for any R whereas (A1) is satisfied if and only if

$$\sum_{l \neq 0} f(R^2|1 - z^l|^2)(1 - z^l) + \sum_{l \neq 0} h(R^2|1 - z^l|^2) \cos(2\pi l/N)(1 - z^l) = 0, \quad (\text{A4})$$

which gives an expression for R . For the specific choice (A3), using the identities

$$\sum_{l \neq 0} \frac{1}{1 - z^l} = \frac{N-1}{2}, \quad \sum_{l \neq 0} \frac{z^l + z^{-l}}{1 - z^{-l}} = -1, \quad (\text{A5})$$

Eq. (A4) reduces to Eq. (7).

We now consider the perturbations

$$x_k(t) = Rz^k + u_k(t); \quad \theta_k = 2\pi k/N + v_k(t).$$

Substituting into the governing equations and linearizing gives

$$u'_k = \sum_j [f'(|x_k - x_j|^2) + \cos(\theta_k - \theta_j)h'(|x_k - x_j|^2)](x_k - x_j)^2(\overline{u_k - u_j}) - J \sin(\theta_k - \theta_j)h(|x_k - x_j|^2)(x_k - x_j)(v_k - v_j) + \sum_j \left[\begin{aligned} & f(|x_k - x_j|^2) + f'(|x_k - x_j|^2)|x_k - x_j|^2 + \cos(\theta_k - \theta_j)h(|x_k - x_j|^2) \\ & + \cos(\theta_k - \theta_j)h'(|x_k - x_j|^2)|x_k - x_j|^2 \end{aligned} \right] (u_k - u_j)$$

and

$$v'_k = \sum_j \sin(\theta_k - \theta_j)g'(|x_k - x_j|^2)\{(x_k - x_j)(\overline{u_k - u_j}) + (\overline{x_k - x_j})(u_k - u_j)\} + \sum_j \cos(\theta_k - \theta_j)g(|x_k - x_j|^2)\{v_k - v_j\}.$$

Following [41,69,75], we use the self-consistent *Ansatz*

$$u_k(t) = A(t)z^{mk+k} + \bar{B}(t)z^{-mk+k}, \\ v_k = C(t)z^{mk} + \bar{C}(t)z^{-mk}.$$

After much algebra, and collecting like terms in z^{mk} and z^{-mk} , we obtain a 3×3 linear system for each mode m :

$$\begin{pmatrix} A' \\ B' \\ C' \end{pmatrix} = \begin{pmatrix} M_{11} & M_{12} & M_{13} \\ M_{21} & M_{22} & M_{23} \\ M_{31} & M_{32} & M_{33} \end{pmatrix} \begin{pmatrix} A \\ B \\ C \end{pmatrix}, \quad (\text{A6})$$

where

$$M_{11} = \sum \left[\begin{aligned} & f(R^2|1 - z^l|^2) + f'(R^2|1 - z^l|^2)R^2|1 - z^l|^2 \\ & + \cos\left(\frac{2\pi l}{N}\right)[h(R^2|1 - z^l|^2) + h'(R^2|1 - z^l|^2)R^2|1 - z^l|^2] \end{aligned} \right] (1 - z^{(m+1)l}), \\ M_{12} = \sum \left[f'(R^2|1 - z^l|^2) + \cos\left(\frac{2\pi l}{N}\right)h'(R^2|1 - z^l|^2) \right] R^2(1 - z^l)^2(1 - z^{(m-1)l}), \\ M_{13} = \sum h(R^2|1 - z^l|^2) \sin(2\pi l/N)R(1 - z^l)(1 - z^{ml})$$

and

$$M_{21} = M_{12}, \\ M_{22} = \sum \left[\begin{aligned} & f(R^2|1 - z^l|^2) + f'(R^2|1 - z^l|^2)R^2|1 - z^l|^2 \\ & + \cos\left(\frac{2\pi l}{N}\right)[h(R^2|1 - z^l|^2) + h'(R^2|1 - z^l|^2)R^2|1 - z^l|^2] \end{aligned} \right] (1 - z^{(m-1)l}), \\ M_{23} = \sum \sin\left(\frac{2\pi l}{N}\right)h(R^2|1 - z^l|^2)R(1 - z^{-l})(1 - z^{ml})$$

and

$$\begin{aligned} M_{31} &= \sum -\sin(2\pi l/N)g'(R^2|1-z^l|^2)\{R(1-z^{-l})(1-z^{(m+1)l})\}, \\ M_{32} &= \sum -\sin(2\pi l/N)g'(R^2|1-z^l|^2)\{R(1-z^l)(1-z^{(m-1)l})\}, \\ M_{33} &= \sum \cos(2\pi l/N)g(R^2|1-z^l|^2)(1-z^{ml}), \end{aligned}$$

where all sums are over $l = 1 \dots N-1$. Specializing to (A3), we use the following key identity:

$$\sum_{l=1}^{N-1} \frac{z^{ml}}{(1-z^l)^2} = \begin{cases} \frac{1}{12} + \frac{1}{24}N^2 - \frac{1}{2}(m-1-N/2)^2, & m \in (1, N-1) \\ -\frac{1}{12}(N-5)(N-1), & m \equiv 0. \end{cases}$$

The expressions for M then become

$$\begin{aligned} M &= \begin{bmatrix} -N + J_1 \frac{N}{2} & \frac{(N-3)(1-J_2)}{2R^2} & 0 \\ \frac{(N-3)(1-J_2)}{2R^2} & \frac{N}{2}J_1 - N & 0 \\ 0 & 0 & 0 \end{bmatrix}, \quad m = 0 \\ M &= \begin{bmatrix} -N & \frac{(N-4)(1-J_2)}{R^2} & i\frac{N}{2}\left(2RJ_1 + \frac{J_2}{R}\right) \\ \frac{(N-4)(1-J_2)}{R^2} & 0 & 0 \\ -i(N-2)\frac{K}{2R^3} & 0 & \frac{K}{2R^2} \end{bmatrix}, \quad m = 1 \\ M &= \begin{bmatrix} -N & \frac{3(N-5)(1-J_2)}{2R^2} & i\frac{N}{2}\left(RJ_1 + \frac{J_2}{R}\right) \\ \frac{3(N-5)(1-J_2)}{2R^2} & \frac{N}{2}J_1 - N & -i\frac{N}{2}\left(2RJ_1 + \frac{J_2}{R}\right) \\ -iK\frac{(N-3)}{R^3} & iK\frac{(N-2)}{2R^3} & -\frac{K}{2R^2}(N-4) \end{bmatrix}, \quad m = 2. \end{aligned}$$

For $m \in (2, N-2)$, we have

$$M = \begin{bmatrix} -N & \frac{(m-1)(-m+N-1)(-J_2+1)}{2R^2} & i\frac{N}{2}\left(RJ_1 + \frac{J_2}{R}\right) \\ \frac{(m-1)(-m+N-1)(-J_2+1)}{2R^2} & -N & -i\frac{N}{2}\left(RJ_1 + \frac{J_2}{R}\right) \\ -K\frac{i}{2R^3}(N-m-1)m & K\frac{i}{2R^3}(m-1)(N-m) & -\frac{K}{2R^2}(N(m-1)-m^2) \end{bmatrix}.$$

It turns out that the modes $m = 0, 1, 2$ are stable in the relevant regimes so we do not examine them here. We have checked this analytically for $K = 0$, but for $K \neq 0$, we were only able to do this numerically. As we will show, however, the expression for $m \in (2, N-2)$ leads to closed form expressions for critical parameters, values that match simulations, so we confine our attention there hereafter. The above matrix [i.e., for $m \in (2, N-2)$] has the following form:

$$M = \begin{bmatrix} a & b & ic \\ b & a & -ic \\ iKd & iKe & Kf \end{bmatrix}, \quad (\text{A7})$$

where

$$\begin{aligned} a &= -N, \quad b = \frac{(m-1)(-m+N-1)(-J_2+1)}{2R^2}, \\ c &= \frac{N}{2}\left(RJ_1 + \frac{J_2}{R}\right), \quad d = \frac{-(N-m-1)m}{2R^3}, \\ e &= \frac{(m-1)(N-m)}{2R^3}, \quad f = \frac{m^2 - N(m-1)}{2R^2}. \end{aligned} \quad (\text{A8})$$

Computing the characteristic polynomial, we find that one of the eigenvalues is given by

$$\lambda_0 = a + b \quad (\text{A9})$$

while the other two are roots of the quadratic

$$K[f(a-b) + c(d-e)] + \lambda(b-a-Kf) + \lambda^2 = 0. \quad (\text{A10})$$

We remind the reader that these expressions are for $m \in (2, N-2)$. This requires $N > 4$. Thus, the following analysis holds only when this condition is met.

From the expressions of the eigenvalues we deduce the instabilities that can occur. There are three types: either (A9) crosses through zero, (A10) crosses through zero, or (A10) exhibits a Hopf bifurcation. These three possibilities correspond to $a+b=0$, $K[f(a-b)+c(d-e)]=0$, and $b-a-Kf=0$ (with $K[f(a-b)+c(d-e)] < 0$), respectively.

Further analysis shows that the ring is unstable with respect to mode $m = 2$ whenever $K > 0$, regardless of the values of J_1, J_2 . Hence, we ignore this boring part of parameter space and consider only the region $K \leq 0$. It turns out that the most unstable mode corresponds to the highest mode $m = \lfloor N/2 \rfloor$. With this choice of m , let J_{1a} be the value of J_1 such that $a+b=0$, and let J_{1b} be the value J_1 such that $f(a-b)+c(d-e)=0$. Finally, let K_{Hopf} be the value of K for which $b-a-Kf=0$. These values are given by (8), (9), and (10) in the main text, respectively. Further analysis shows that

$J_{1a} < J_{1b}$. (Note the swarmalators execute oscillations in both space and phase after the Hopf bifurcation.)

The stability diagram is illustrated in Fig. 2. Suppose that $K \leq 0$. Then, for J_1 below J_{1a} , the ring is unstable with respect to spatial perturbation. For $J_{1a} < J_1 < J_{1b}$, the ring is unstable with respect to a mixture of spatial and phase perturbations, when $K < 0$, but is stable when $K = 0$. Finally, the ring is fully stable if $J_{1b} < J_1$ as long as $K_{\text{Hopf}} < K < 0$. This stability region is indicated in green in Fig. 2.

APPENDIX B: DENSITY OF ANNULAR PHASE WAVE STATE

The density of swarmalators in the annular phase wave state (best expressed in polar coordinates) is given by

$$\rho(r, \phi, \theta) = \frac{1}{2\pi} g(r) \delta(\phi - \theta), \quad R_1 \leq r \leq R_2 \quad (\text{B1})$$

$$= 0, \quad \text{elsewhere} \quad (\text{B2})$$

where r_k, ϕ_k is the radial position and spatial angle of the k th swarmalator, and $g(r), R_1, R_2$ are unknowns to be solved for. We first solve for $g(r)$, which in turn lets us solve for R_1, R_2 .

1. Find radial density $g(r)$

Swarmalators are stationary (in both space and phase) in the annular phase wave state:

$$\underline{v} \equiv 0, \quad (\text{B3})$$

where we have introduced the ‘‘underline’’ notation $\underline{v} = (\mathbf{v}_x, v_\theta)$ (so that $\underline{v} \in \mathbb{R}^3$, $\mathbf{v}_x \in \mathbb{R}^2$, and $v_\theta \in \mathbb{R}$). By applying the divergence operator to (B3) we generate another equation

$$\nabla \cdot \underline{v} \equiv 0. \quad (\text{B4})$$

Equations (B3) and (B4) let us solve for $g(r)$, as we will now show.

Zero divergence condition. We first investigate Eq. (B4). In polar coordinates the continuum expressions for the velocity \underline{v} are

$$v_r = \int (s \cos(\phi' - \phi) - r) \left(1 + J_1 \cos(\theta' - \theta) - \frac{1 - J_2 \cos(\theta' - \theta)}{s^2 - 2rs \cos(\theta' - \theta) + r^2} \right) s \rho(s, \phi', \theta') ds d\phi' d\theta', \quad (\text{B5})$$

$$v_\phi = \int s \sin(\phi' - \phi) \left(1 + J_1 \cos(\theta' - \theta) - \frac{1 - J_2 \cos(\theta' - \theta)}{s^2 - 2rs \cos(\theta' - \theta) + r^2} \right) s \rho(s, \phi', \theta') ds d\phi' d\theta', \quad (\text{B6})$$

$$v_\theta = K \int \frac{\sin(\theta' - \theta)}{s^2 - 2rs \cos(\phi' - \phi) + r^2} s \rho(s, \phi', \theta') ds d\phi' d\theta', \quad (\text{B7})$$

where $v_\phi = r\dot{\theta}$. Substituting the Ansatz (B1) for the density ρ into the velocity fields above leads to $v_\phi = v_\theta = 0$. The radial

component becomes

$$v_r = \frac{1}{2\pi} \int_{R_1}^{R_2} \int_{-\pi}^{\pi} (s \cos \beta - r) g(r) s ds d\beta - \frac{1}{2\pi} \int_{R_1}^{R_2} \int_{-\pi}^{\pi} \frac{s \cos(\beta) - r}{s^2 - 2rs \cos \beta + r^2} g(s) s ds d\beta + \frac{J_1}{2\pi} \int_{R_1}^{R_2} \int_{-\pi}^{\pi} (s \cos^2 \beta - r \cos \beta) g(s) s ds d\beta + \frac{J_2}{2\pi} \int_{R_1}^{R_2} \int_{-\pi}^{\pi} \frac{s \cos^2 \beta - r \cos \beta}{s^2 - 2rs \cos \beta + r^2} g(s) s ds d\beta, \quad (\text{B8})$$

where $\beta = \phi' - \phi$. Evaluating the first and third integrals is elementary, while the second and fourth can be computed using Poisson's formula

$$\frac{1}{2\pi} \int_{-\pi}^{\pi} \frac{\cos m\theta}{s^2 - 2r \cos \theta + r^2} d\theta = \begin{cases} \left(\frac{r}{s}\right)^m \frac{1}{s^2 - r^2} & \text{if } r < s, \\ \left(\frac{s}{r}\right)^m \frac{1}{r^2 - s^2} & \text{if } r > s. \end{cases} \quad (\text{B9})$$

The result is

$$v_r = -r \int_{R_1}^{R_2} g(s) s ds + \frac{1}{r} \int_0^r s g(s) ds + \frac{J_1}{2} \int_{R_1}^{R_2} s^2 g(s) ds + \frac{J_2}{2} \int_r^\infty g(s) ds - \frac{J_2}{2r^2} \int_0^r s^2 g(s) ds. \quad (\text{B10})$$

In polar coordinates the divergence is

$$\nabla \cdot \underline{v} = \frac{1}{r} \frac{\partial}{\partial r} (r v_r) + \frac{1}{r} \frac{\partial}{\partial \phi} (v_\phi) + \frac{\partial}{\partial \theta} (v_\theta). \quad (\text{B11})$$

Since $v_\phi = v_\theta = 0$ this reduces to

$$\nabla \cdot \underline{v} = \frac{1}{r} \frac{\partial}{\partial r} (r v_r). \quad (\text{B12})$$

Substituting v_r as per (B10) into the above expression and applying the derivative operator gives

$$\nabla \cdot \underline{v} = \frac{1}{r} \left(-2r \int_{R_1}^{R_2} g(s) s ds + r g(r) (1 - J_2) + \frac{J_1}{2} \int_0^\infty s^2 g(s) ds + \frac{J_2}{2} \int_r^\infty g(s) s^2 ds - \frac{J_2}{2r^2} \int_0^r s^2 g(s) ds \right). \quad (\text{B13})$$

Setting this to zero, as required by (B4), and rearranging, leads to the following integral equation for $g(r)$:

$$g(r) = \frac{1}{1 - J_2} \left(2 - \frac{J_1}{2r} \int_{R_1}^{R_2} s^2 g(s) ds - \frac{J_2}{r} \int_r^{R_2} g(s) ds - \frac{J_2}{r^3} \int_{R_1}^r s^2 g(s) ds \right). \quad (\text{B14})$$

Solve integral equation. We solve the above integral equation for $g(r)$ by reducing it to an ODE. Multiplying both sides

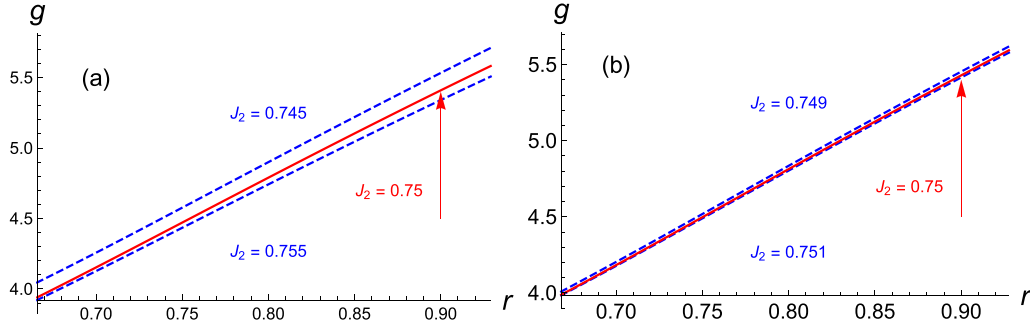


FIG. 6. Radial density $g(r)$ for $J_1 = 0.5$ for values of J_2 in a neighborhood of 0.75. Blue dashed lines show are for $J_2 \neq 3/4$ calculated using expression (B18). The red solid line is for $J_2 = 3/4$ using expression (B22). The density $g(r)$ varies smoothly as J_2 passes through 0.75. Panel (a) shows values $J_2 = 0.745, 0.755$, which hug the curve at $J_2 = 0.75$. In panel (b) we use a tighter neighborhood with extremal values 0.749, 0.751, which produces a tighter ‘hugging’. These results indicate that there is no change in the behavior of $g(r)$ at the value $J_2 = 0.75$.

by r^3 and taking a derivative with respect to r gives

$$3r^2 g(r) + r^3 g'(r) = \frac{1}{1-J_2} \left[6r^2 - J_2 r \int_r^\infty g(s) ds + J_1 r \int_{R_1}^{R_2} s^2 g(s) ds \right]. \quad (\text{B15})$$

We next divide by r to give

$$3r g(r) + r^2 g'(r) = \frac{1}{1-J_2} \left[6r - J_2 \int_r^\infty g(s) ds + J_1 \int_{R_1}^{R_2} s^2 g(s) ds \right] \quad (\text{B16})$$

since this expression is easier to differentiate, as there then are only constants in front of the integrals. Taking the derivative

then leads the following simple, second order ODE for $g(r)$:

$$r^2 g''(r) + 5r g'(r) + \left(3 - \frac{J_2}{1-J_2} \right) g(r) - \frac{6}{1-J_2} = 0. \quad (\text{B17})$$

The solution to this equation is

$$g(r) = C_1 r^{-\frac{1}{\sqrt{1-J_2}-2}} + C_2 r^{\frac{1}{\sqrt{1-J_2}-2}} + \frac{6}{3-4J_2}. \quad (\text{B18})$$

We find the constants of integration C_1, C_2 by substituting this back into the integral equation (B14), which gives

$$\frac{A}{r} + \frac{B}{r^3} = 0, \quad (\text{B19})$$

where A, B are complex functions of $C_1, C_2, R_1, R_2, J_1, J_2$ that must be identically 0. Enforcing this constraint leads to the following complicated expressions for C_1, C_2 :

$$C_1 = -\frac{2R_1^{\frac{1}{\sqrt{1-J_2}}} R_2^{\frac{1}{\sqrt{1-J_2}}} \left[J_1 (\sqrt{1-J_2}-1) R_2^2 (R_2^2 R_1^{\frac{1}{\sqrt{1-J_2}}} - R_1^2 R_2^{\frac{1}{\sqrt{1-J_2}}}) + J_2 (3(\sqrt{1-J_2}-1) R_2^2 R_1^{\frac{1}{\sqrt{1-J_2}}} + (\sqrt{1-J_2}+1) R_1^2 R_2^{\frac{1}{\sqrt{1-J_2}}}) \right]}{\sqrt{1-J_2}(4J_2-3) \left((-J_1 R_2^2 + J_2 + 2\sqrt{1-J_2}-2) R_1^{\frac{2}{\sqrt{1-J_2}}} + R_2^{\frac{2}{\sqrt{1-J_2}}} (J_1 R_2^2 - J_2 + 2\sqrt{1-J_2}+2) \right)} \quad (\text{B20})$$

$$C_2 = -\frac{2J_2 \left((-J_1 R_2^2 + J_2 + 2\sqrt{1-J_2}-2) R_1^{\frac{1}{\sqrt{1-J_2}+2}} + R_2^{\frac{1}{\sqrt{1-J_2}+2}} (J_1 R_2^2 + 3J_2) \right)}{(\sqrt{1-J_2}-1) \sqrt{1-J_2} (4J_2-3) \left((-J_1 R_2^2 + J_2 + 2\sqrt{1-J_2}-2) R_1^{\frac{2}{\sqrt{1-J_2}}} + R_2^{\frac{2}{\sqrt{1-J_2}}} (J_1 R_2^2 - J_2 + 2\sqrt{1-J_2}+2) \right)}. \quad (\text{B21})$$

Looking at the third term in Eq. (B18), we see the value $J_2 = \frac{3}{4}$ is problematic. Why is this value distinguished? The reason is that the third term in the ODE (B17) for $g(r)$ becomes zero at this value of J_2 . In this case, $g(r), C_1$, and C_2 are given by

$$g(r) = -\frac{C_1}{4r^4} + C_2 + 6 \ln r, \quad J_2 = \frac{3}{4}, \quad (\text{B22})$$

$$C_1 = \frac{8R_1^4 R_2^4 \left((4J_1 R_2^2 + 9) \ln R_1 - (4J_1 R_2^2 + 9) \ln R_2 + 6 \right)}{-4J_1 R_2^6 + 4J_1 R_1^4 R_2^2 - 9R_2^4 + R_1^4} \quad (\text{B23})$$

$$C_2 = \frac{2 \left(-4J_1 R_2^6 + 4J_1 R_1^4 R_2^2 + 3R_2^4 (4J_1 R_2^2 + 9) \ln R_2 - 3R_1^4 (4J_1 R_2^2 + 1) \ln R_1 - 27R_2^4 + R_1^4 \right)}{-4J_1 R_2^6 + 4J_1 R_1^4 R_2^2 - 9R_2^4 + R_1^4}. \quad (\text{B24})$$

The difference between the expressions (B18) and (B22) for $g(r)$ are superficial. By this we mean there is no change in the physical behavior of the swarmalator system as J_2 passes

through $\frac{3}{4}$. We demonstrate this two ways. The first way is by observing that R_1, R_2 vary smoothly with respect to J_2 as drawn in Fig. 3; no change in behavior occurs at $J_2 = \frac{3}{4}$. The

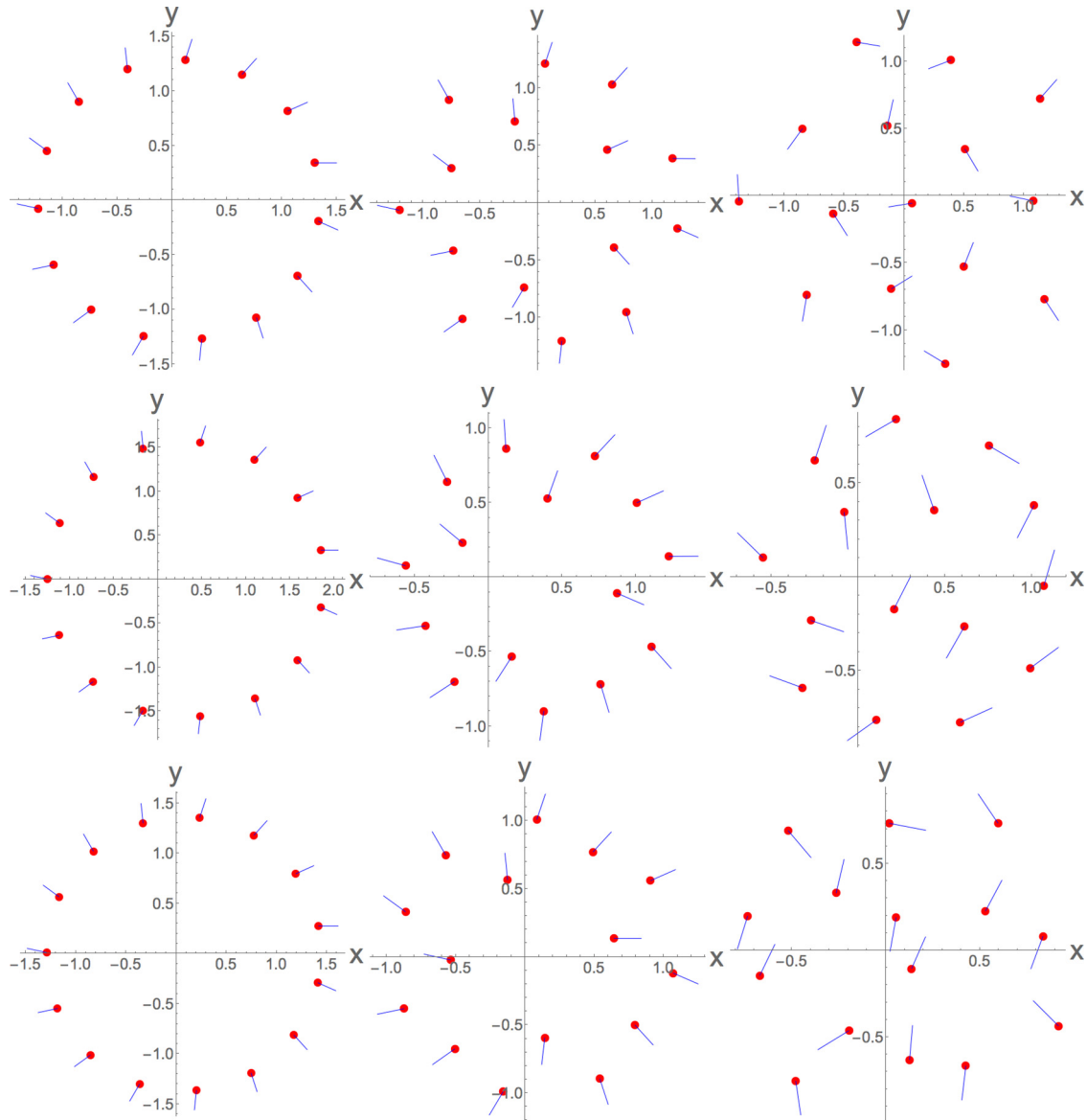


FIG. 7. States found with difference choices of the functions (23), (24), and (25). Simulations for all plots were for $N = 15$ swarmalators, and the Euler method with a step size of $dt = 0.01$ and $N_t = 5 \times 10^5$ number of time steps was used. The top row is for choice (23), the second for choice (24), and the third for choice (25). The ring state, corresponding to subfigure B in the stability diagram in Fig. 2, is shown in the first column. Reading from top to bottom, the parameter values were $(J_1, J_2, K) = (2.7, 0, -0.001)$, $(1, 0, 0, -0.01)$, $(1.5, 0, -0.001)$. The fattened ring state, corresponding to subfigure E in Fig. 2, is shown in the second column. Parameter values were $(J_1, J_2, K) = (1.5, 0, -0.001)$, $(0.2, 0, 0, -0.01)$, $(0.8, 0, -0.001)$. The column shows the nonstationary state depicted in subfigure G in Fig. 2. Parameter values were $(J_1, J_2, K) = (1.5, 0, -5)$, $(0.2, 0, 0, -2)$, $(0.8, 0, 5)$. Note, in this last column, the swarmalators move around erratically in both space and phase.

second way is by plotting $g(r)$ at the values for values of J_2 is the neighborhood of $\frac{3}{4}$ in Fig. 6. As can be seen $g(r)$ varies smooth as J_2 is varied through $\frac{3}{4}$. Hence, the value of $J_2 = \frac{3}{4}$ has no physical significance.

2. Inner and outer radii

So far we have solved for $g(r)$ using the zero divergence condition (B4). The zero velocity condition (B3) must also be

satisfied. We here check the condition $v_r = 0$, and show that along with mass conservation $\int \rho(x, \theta) dx d\theta = 1$, it also lets us determine the inner and outer radii R_1, R_2 .

Zero velocity condition. Substituting the expression (B18) for $g(r)$ into Eq. (B10) for v_r leads to

$$v_r = \frac{h_1(R_1, R_2, J_1, J_2)}{r}, \tag{B25}$$

where h_1 is given by

$$\begin{aligned}
h_1 = & [2J_2^2(2\sqrt{J_2+1} + 3R_2^2 - 6) + J_2\{R_2^2[J_1(4\sqrt{J_2+1} - 2R_2^2 - 4) - 15\sqrt{J_2+1} + 21] + 19\sqrt{J_2+1} - 25\} \\
& + (\sqrt{J_2+1} - 1)(J_1R_2^4 + 3(J_1 - 4)R_2^2 + 12)]R_1^{\frac{2}{\sqrt{J_2+1}}} + 4(J_2 - \sqrt{J_2+1} + 1)R_2^{\frac{1}{\sqrt{J_2+1}}}(J_1R_2^2 + J_2)R_1^{\frac{1}{\sqrt{J_2+1}}+2} \\
& + [J_2(-2J_1R_2^2 + 7\sqrt{J_2+1} - 13) + 3(\sqrt{J_2+1} - 1)(J_1R_2^2 + 4) - 2J_2^2]R_1^{\frac{2}{\sqrt{J_2+1}}+2} + 4(-J_2 + \sqrt{J_2+1} - 1)R_2^{\frac{1}{\sqrt{J_2+1}}+2} \\
& \times (3J_2 - J_1R_2^2)R_1^{\frac{1}{\sqrt{J_2+1}}} - R_1^2R_2^{\frac{2}{\sqrt{J_2+1}}}[J_2(2J_1R_2^2 + 3\sqrt{J_2+1} + 3) - J_1(\sqrt{J_2+1} - 1)R_2^2 + 2J_2^2] \\
& - R_2^{\frac{2}{\sqrt{J_2+1}}}[J_2^2(4\sqrt{J_2+1} - 6R_2^2 + 4) + J_2\{R_2^2[2J_1(2\sqrt{J_2+1} + R_2^2 - 2) - 3(\sqrt{J_2+1} + 1)] + 3(\sqrt{J_2+1} + 1)\} \\
& - 3J_1(\sqrt{J_2+1} - 1)R_2^2(R_2^2 - 1)]. \tag{B26}
\end{aligned}$$

We require $v_r = 0$ for all r , which implies $h_1(R_1, R_2, J_1, J_2) = 0$.

Mass conservation. The density Ansatz (B1) must also be normalized: $\int \rho(x, \theta) dx d\theta = 1$. This leads to a second equation $h_2(R_1, R_2, J_1, J_2) = 0$ where

$$\begin{aligned}
h_2 = & - [J_2(2J_1R_2^2 + 3\sqrt{J_2+1} + 3) - J_1(\sqrt{J_2+1} - 1)R_2^2 + 2J_2^2]R_1^2R_2^{\frac{2}{\sqrt{J_2+1}}} \\
& + 4(-J_2 + \sqrt{J_2+1} - 1)R_1^{\frac{1}{\sqrt{J_2+1}}}(3J_2 - J_1R_2^2)R_2^{\frac{1}{\sqrt{J_2+1}}+2} \\
& + [J_2(-2J_1R_2^2 + 7\sqrt{J_2+1} - 13) + 3(\sqrt{J_2+1} - 1)(J_1R_2^2 + 4) - 2J_2^2]R_1^{\frac{2}{\sqrt{J_2+1}}+2}. \tag{B27}
\end{aligned}$$

Thus, we have derived the following set of simultaneous equations whose roots determine R_1, R_2 in terms of the parameters J_1 and J_2 :

$$h_1(R_1, R_2, J_1, J_2) = 0, \tag{B28}$$

$$h_2(R_1, R_2, J_1, J_2) = 0. \tag{B29}$$

APPENDIX C: GENERICITY

In Fig. 7 we show the states shown in Fig. 2 found when different functional forms [enumerated by (23), (24), (25)] are chosen for $\mathbf{I}_1, \mathbf{I}_2, F, G$ (see Sec. III D). As can be seen, all states are recovered.

-
- [1] A. Pikovsky, M. Rosenblum, and J. Kurths, *Synchronization: A Universal Concept in Nonlinear Sciences* (Cambridge University Press, Cambridge, 2003).
- [2] S. H. Strogatz, *Phys. D (Amsterdam)* **143**, 1 (2000).
- [3] A. T. Winfree, *The Geometry of Biological Time* (Springer, Berlin, 2001).
- [4] A. T. Winfree, *J. Theor. Biol.* **16**, 15 (1967).
- [5] C. S. Peskin, *Mathematical Aspects of Heart Physiology* (Courant Institute of Mathematical Sciences, New York University, 1975).
- [6] C. Liu, D. R. Weaver, S. H. Strogatz, and S. M. Reppert, *Cell* **91**, 855 (1997).
- [7] J. B. Buck, *Q. Rev. Biol.* **13**, 301 (1938).
- [8] J. Buck, *Q. Rev. Biol.* **63**, 265 (1988).
- [9] I. Aihara, S. Horai, H. Kitahata, K. Aihara, and K. Yoshikawa, *IEICE Trans. Fundamentals Electron. Commun. Comput. Sci.* **90**, 2154 (2007).
- [10] I. Aihara, H. Kitahata, K. Yoshikawa, and K. Aihara, *Artificial Life Robotics* **12**, 29 (2008).
- [11] I. Aihara, *Phys. Rev. E* **80**, 011918 (2009).
- [12] J. Aldridge and E. K. Pye, *Nature (London)* **259**, 670 (1976).
- [13] K. Wiesenfeld, P. Colet, and S. H. Strogatz, *Phys. Rev. Lett.* **76**, 404 (1996).
- [14] A. E. Motter, S. A. Myers, M. Anghel, and T. Nishikawa, *Nat. Phys.* **9**, 191 (2013).
- [15] S. H. Strogatz, D. M. Abrams, A. McRobie, B. Eckhardt, and E. Ott, *Nature (London)* **438**, 43 (2005).
- [16] I. D. Couzin, J. Krause, R. James, G. D. Ruxton, and N. R. Franks, *J. Theor. Biol.* **218**, 1 (2002).
- [17] I. D. Couzin and J. Krause, *Adv. Study Behav.* **32**, 1 (2003).
- [18] I. Couzin, *Nature (London)* **445**, 715 (2007).
- [19] J. E. Herbert-Read, *J. Exp. Biol.* **219**, 2971 (2016).
- [20] D. J. Sumpter, *Collective Animal Behavior* (Princeton University Press, Princeton, NJ, 2010).
- [21] A. Mogilner and L. Edelstein-Keshet, *J. Math. Biol.* **38**, 534 (1999).
- [22] A. Mogilner, L. Edelstein-Keshet, L. Bent, and A. Spiros, *J. Math. Biol.* **47**, 353 (2003).
- [23] R. Lukeman, Y.-X. Li, and L. Edelstein-Keshet, *Proc. Natl. Acad. Sci. USA* **107**, 12576 (2010).
- [24] A. J. Bernoff and C. M. Topaz, *SIAM Rev.* **55**, 709 (2013).
- [25] R. C. Fetecau, Y. Huang, and T. Kolokolnikov, *Nonlinearity* **24**, 2681 (2011).

- [26] W. Bialek, A. Cavagna, I. Giardina, T. Mora, E. Silvestri, M. Viale, and A. M. Walczak, *Proc. Natl. Acad. Sci. USA* **109**, 4786 (2012).
- [27] M. Ballerini, N. Cabibbo, R. Candelier, A. Cavagna, E. Cisbani, I. Giardina, V. Lecomte, A. Orlandi, G. Parisi, A. Procaccini *et al.*, *Proc. Natl. Acad. Sci. USA* **105**, 1232 (2008).
- [28] L. Edelstein-Keshet, J. Watmough, and D. Grunbaum, *J. Math. Biol.* **36**, 515 (1998).
- [29] C. M. Topaz, A. J. Bernoff, S. Logan, and W. Toolson, *Eur. Phys. J. Spec. Top.* **157**, 93 (2008).
- [30] J. Buhl, D. J. Sumpter, I. D. Couzin, J. J. Hale, E. Despland, E. Miller, and S. J. Simpson, *Science* **312**, 1402 (2006).
- [31] D. L. Levy and T. Requeijo, *Bull. Math. Biol.* **70**, 1684 (2008).
- [32] A. Galante and D. Levy, *Phys. D (Amsterdam)* **260**, 176 (2013).
- [33] P.-C. Chavy-Waddy and T. Kolokolnikov, *Nonlinearity* **29**, 3174 (2016).
- [34] Y. Katz, K. Tunstrom, C. C. Ioannou, C. Huepe, and I. D. Couzin, *Proc. Natl. Acad. Sci. USA* **108**, 18720 (2011).
- [35] A. B. Barbaro, K. Taylor, P. F. Trethewey, L. Youseff, and B. Birnir, *Math. Comput. Simul.* **79**, 3397 (2009).
- [36] T. J. Pitcher and C. J. Wyche, in *Predators and Prey in Fishes* (Springer, Berlin, 1983), pp. 193–204.
- [37] Y. Chen and T. Kolokolnikov, *J. R. Soc. Interface* **11**, 20131208 (2014).
- [38] B. Grzybowski, H. Stone, and G. Whitesides, *Nature (London)* **405**, 1033 (2000).
- [39] J. H. Von Brecht, D. Uminsky, T. Kolokolnikov, and A. L. Bertozzi, *Math. Models Methods Appl. Sci.* **22**, 1140002 (2012).
- [40] J. H. von Brecht and D. Uminsky, *J. Nonlinear Sci.* **22**, 935 (2012).
- [41] T. Kolokolnikov, H. Sun, D. Uminsky, and A. L. Bertozzi, *Phys. Rev. E* **84**, 015203 (2011).
- [42] J. H. von Brecht and D. T. Uminsky, *Nonlinearity* **30**, 225 (2016).
- [43] J. Abo-Shaer, C. Raman, J. Vogels, and W. Ketterle, *Science* **292**, 476 (2001).
- [44] T. W. Neely, E. C. Samson, A. S. Bradley, M. J. Davis, and B. P. Anderson, *Phys. Rev. Lett.* **104**, 160401 (2010).
- [45] P. Torres, P. Kevrekidis, D. Frantzeskakis, R. Carretero-González, P. Schmelcher, and D. Hall, *Phys. Lett. A* **375**, 3044 (2011).
- [46] K. S. Fine, A. C. Cass, W. G. Flynn, and C. F. Driscoll, *Phys. Rev. Lett.* **75**, 3277 (1995).
- [47] D. Durkin and J. Fajans, *Phys. Fluids* **12**, 289 (2000).
- [48] M. K. McClintock, *Nature (London)* **229**, 244 (1971).
- [49] K. Uriu, S. Ares, A. C. Oates, and L. G. Morelli, *Phys. Rev. E* **87**, 032911 (2013).
- [50] D. J. Stilwell, E. M. Bollt, and D. G. Roberson, *SIAM J. Appl. Dyn. Syst.* **5**, 140 (2006).
- [51] M. Frasca, A. Buscarino, A. Rizzo, L. Fortuna, and S. Boccaletti, *Phys. Rev. Lett.* **100**, 044102 (2008).
- [52] N. Fujiwara, J. Kurths, and A. Díaz-Guilera, *Phys. Rev. E* **83**, 025101(R) (2011).
- [53] A. Buscarino, L. Fortuna, M. Frasca, and S. Frisenna, *Chaos* **26**, 116302 (2016).
- [54] D. Tanaka, *Phys. Rev. Lett.* **99**, 134103 (2007).
- [55] M. Iwasa, K. Iida, and D. Tanaka, *Phys. Rev. E* **83**, 036210 (2011).
- [56] M. Iwasa, K. Iida, and D. Tanaka, *Phys. Rev. E* **81**, 046220 (2010).
- [57] M. Starnini, M. Frasca, and A. Baronchelli, *Sci. Rep.* **6**, 31834 (2016).
- [58] K. P. O'Keeffe, H. Hong, and S. H. Strogatz, *Nat. Commun.* **8**, 1504 (2017).
- [59] T. J. Walker, *Science* **166**, 891 (1969).
- [60] M. D. Greenfield, *Am. Zool.* **34**, 605 (1994).
- [61] I. Aihara, T. Mizumoto, T. Otsuka, H. Awano, K. Nagira, H. G. Okuno, and K. Aihara, *Sci. Rep.* **4**, 3891 (2014).
- [62] Y. Yang, J. Elgeti, and G. Gompfer, *Phys. Rev. E* **78**, 061903 (2008).
- [63] O. A. Igoshin, A. Mogilner, R. D. Welch, D. Kaiser, and G. Oster, *Proc. Natl. Acad. Sci. USA* **98**, 14913 (2001).
- [64] J. Yan, M. Bloom, S. C. Bae, E. Luijten, and S. Granick, *Nature (London)* **491**, 578 (2012).
- [65] J. H. M. Evers, R. C. Fetecau, and T. Kolokolnikov, *arXiv:1612.08074*.
- [66] J. Yan, K. Chaudhary, S. C. Bae, J. A. Lewis, and S. Granick, *Nat. Commun.* **4**, 1516 (2013).
- [67] T. Havelock, *London, Edinburgh, Dublin Philos. Mag. J. Sci.* **11**, 617 (1931).
- [68] Y. Chen, T. Kolokolnikov, and D. Zhirov, *Proc. R. Soc. A* **469**, 20130085 (2013).
- [69] A. L. Bertozzi, T. Kolokolnikov, H. Sun, D. Uminsky, and J. Von Brecht, *Commun. Math. Sci.* **13**, 955 (2015).
- [70] D. Balagué, J. Carrillo, T. Laurent, and G. Raoul, *Arch. Ration. Mech. Anal.* **209**, 1055 (2013).
- [71] A. Snezhko and I. S. Aranson, *Nat. Mater.* **10**, 698 (2011).
- [72] O. Pohl and H. Stark, *Phys. Rev. Lett.* **112**, 238303 (2014).
- [73] A. Maude, *Nature (London)* **200**, 381 (1963).
- [74] Y. Kuramoto, *Chemical Oscillations, Waves, and Turbulence* (Springer, Berlin, 1984).
- [75] T. Kolokolnikov, P. Kevrekidis, and R. Carretero-González, *Proc. R. Soc. A* **470**, 20140048 (2014).
- [76] G. Albi, D. Balagué, J. Carrillo, and J. Von Brecht, *SIAM J. Appl. Math.* **74**, 794 (2014).